

Detection of polarized Fermi-bubble synchrotron and dust emission

Uri Keshet*

(Dated: January 3, 2024)

The elusive polarized microwave signal from the Fermi bubbles is disentangled from the more extended polarized lobes, which similarly emanate from the Galactic plane but stretch farther west of the bubbles. The $\sim 20\%$ synchrotron polarization reveals magnetic fields preferentially parallel to the bubble edges, as expected downstream of a strong shock. The $\sim 20\%$ polarization of thermal dust emission is similarly oriented, constraining grain alignment in an extreme environment. We argue that the larger lobes arise from an older Galactic-center, likely supermassive black-hole, outburst.

The bipolar Fermi bubbles (FBs), emanating from the center of the Milky Way [1, 2] and extending out to $|b| \gtrsim 50^\circ$ latitudes, each presents as a fairly uniform γ -ray teardrop-shaped structure [3, 4], demarcated by an X-ray shell [5], and coincident with a dust component [6] and with radio low frequency [6] to microwave [7, 8] synchrotron emission which brightens to a haze [9] near the Galactic center (GC). Their morphology, X-ray shells, and integrated [4, 7, 10–12] and edge [13] energy spectra, featuring γ -ray and microwave cooling breaks [6], indicate that the FBs arose a few Myr ago, as outflows from the super-massive black hole (SMBH), which must have been collimated [14] nearly perpendicular to the Galactic plane [15], and identify the FB edges as strong, Mach $\gtrsim 5$ forward shocks [6, 13].

The anticipated polarized signal from the FBs has drawn much attention, not only as a probe of their magnetic fields and associated physical processes, but also due to their alleged relation to pronounced, extended polarized lobes [16, 17] that similarly emanate from the Galactic plane, as described below. The polarized signal from the bulk of the FBs was argued to be too weak to pick up, directly or through template decomposition, in *WMAP* [18, 19] and *Planck* [8, 20] maps. However, a local linearly-polarized signal is anticipated just inside the FB edges, as the shock compresses or otherwise amplifies magnetic fields, relativistic particles, and dust. As magnetic fields \mathbf{B} are preferentially amplified parallel to shock fronts, a downstream polarized component $\theta \perp \mathbf{B}$ is expected perpendicular to the FB edges, in both synchrotron and thermal-dust emission.

We thus focus on the vicinity of the FB edges, identified by gradient filters [13], and bin the polarized microwave data parallel to the edge in the same method previously used to measure the γ -ray [13], X-ray [5], and radio [6] spectra in the near downstream. In particular, we adopt the coarse-grained [13] edges of the FBs, well-confining their signature in the 3–30 GeV, 15-year *Fermi*-LAT data [6] used here.

By focusing on the known FB edges, we avoid confusion with the aforementioned extended polarized lobes, observed in 23 GHz *WMAP* [16] and 2.3 GHz S-PASS

[17] data. Figure 1 shows the γ -ray (red) FB edges (dot-dashed orange curves [13]), and the polarized synchrotron (green) lobe putative [21] edges (double-dot dashed green curves [17]). The polarized lobes, partly overlapping the east edges of the FBs, were tentatively identified with the bubbles, despite their different morphology.

There are, however, several reasons to doubt this lobe–FB association, and test it using the FB edges. First, the lobes extend far beyond the west edges of the FBs, so

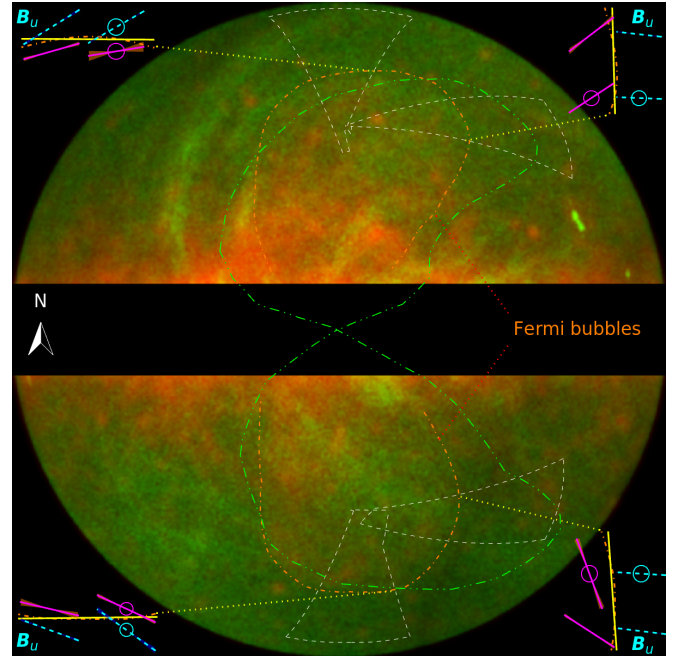


FIG. 1. False-color image of γ -ray (3–30 GeV *Fermi*-LAT; red) and polarized microwave (23 GHz *WMAP*; green) intensities in an orthographic projection; the bright, $|b| \lesssim 5^\circ$ Galactic plane is masked. The polarized lobes (with putative edges [17] shown as double-dot-dashed green curves) extend west of the FBs (edges [13] in dot-dashed orange). For each of the four sectors analyzed (dashed white boundaries), we show (in the respective image corner) the FB edge in a Cartesian projection, along with its mean orientation (solid yellow line) and the directions of the projected upstream (cyan dashed lines with shaded dispersion) and downstream excess (solid magenta with orange dispersion) magnetic fields, as inferred from synchrotron (*Planck* 30 GHz) and dust (*Planck* 353 GHz; denoted by circles) polarizations.

* Physics Department, Ben-Gurion University of the Negev, POB 653, Be'er-Sheva 84105, Israel; ukeshet@bgu.ac.il

they could not arise from the same outburst that drove the FB forward shocks. A similar argument holds for the shear size of the lobes, spanning a solid angle $\gtrsim 40\%$ larger than the FBs. Second, the lobes are far less east-west symmetric than the FBs, presenting a much stronger westward curvature with increasing $|b|$. Third, the lobe ridges are traced down to the $|b| \simeq 10^\circ$ depolarization limit, where they already reach longitudes $l \gtrsim 10^\circ$ east of the GC [17]; therefore, the lobes either emanate far east of the GC, or emanate from the GC but initially head east before sharply curving back west at $|b| < 10^\circ$, unlike the FBs. Finally, the polarization orientation is approximately perpendicular to the ridges, with position angles $0 \lesssim \mp\theta(\pm b \gtrsim 10^\circ) \lesssim 30^\circ$ (θ measured south due east, in *WMAP* conventions [22]; henceforth), showing little correlation with the FBs.

We search for the linearly polarized signal from the FBs at high, $|b| > 30^\circ$ latitudes, where depolarization effects and confusion with Galactic structures diminish. The FB outskirts, where polarization is expected, are examined in four different sectors, marked (by dashed white boundaries) in Fig. 1. In each hemisphere, we choose one sector at the high-latitude tip of the bubble, and one sector on its west side; the eastern FB edges are avoided due to possible confusion with the putative lobe edges. Although wide sectors would provide a better signal-to-noise ratio, we adopt fairly narrow sectors, along which the projected FB edge is approximately linear, in order to better pick up the polarized signal with a meaningful polarization angle.

Figure 1 summarizes, for each sector (in its respective corner, using a Cartesian projection), the local FB edge morphology, its approximate orientation, and the inferred directions of the projected upstream (dashed cyan) and downstream excess (solid magenta) magnetic fields, based on both synchrotron and thermal dust (marked by circles) emission. The FB polarization properties in each sector, including these inferred magnetic field orientations, are derived from the radial (Fig. 2) and spectral (Fig. 3) profiles of the cosmic microwave background (CMB)-subtracted brightness I in *WMAP* and *Planck*, full-mission, maps [6], along with their Q and U counterparts, where I , Q , and U are Stokes parameters.

Figure 2 demonstrates the radial profiles of γ -ray and microwave signals measured near the FB edge in each of the four sectors, stacked at different angular distances ψ from the edge. Here, ψ increases outward, away from the GC, so the shock upstream (downstream) lies at $\psi \gtrsim 0$ ($\psi \lesssim 0$). Foregrounds typically vary slowly with ψ at the high latitudes and large angular scales of interest, and so can be approximated using their mean upstream value; the figure shows differences (denoted by Δ ; circles and squares) with respect to such fixed foreground estimates.

The brightness I was previously found to abruptly rise as one crosses the FB edge downstream, in γ -rays [13], X-rays [5], and microwaves [6]. Figure 2 shows a similar rise in the linearly-polarized microwave amplitude $|L|$

(squares), in all four sectors, where

$$L \equiv Q + iU. \quad (1)$$

The downstream rise in $|L|$ is seen in both synchrotron and dust emission, represented [6] respectively by the lowest (30 GHz; filled symbols) and highest (353 GHz; empty symbols) *Planck* polarization channels. The downstream polarized excess $|\Delta L|$ roughly follows the respective brightness excess ΔI . As the effect is well-localized and far from the radio-lobe edges, especially in the western sectors, we conclude that the ΔL excess is associated with the FBs and not with the lobes.

Figure 3 presents the FB microwave excess in all *WMAP* and *Planck* polarization channels, spanning the $23 < \nu < 353$ GHz frequency range. For each sector, the ΔI (top panels) and ΔL (middle and bottom panels) properties are shown in the near (red diamonds), mid (green squares) and far (blue circles) downstream regions, which are defined in Fig. 2. The top panels and insets confirm that the $\nu \lesssim 50$ GHz and $\nu \gtrsim 100$ GHz ranges are dominated respectively by $\Delta I \propto \nu^{-\alpha}$ synchrotron and $\Delta I \propto \nu^{7/2}/(e^{h\nu/k_B T} - 1)$ thermal dust emission. Here, α is the synchrotron spectral index, T is the dust temperature, h is Planck's constant, and k_B is Boltzmann's constant; for a spectral analysis, see [6].

In both synchrotron and dust regimes, we find (middle panels) a near-downstream linear polarization fraction

$$|\Delta L|/\Delta I \simeq 20\%, \quad (2)$$

in both north and south sectors, in which the foreground is fairly constant and robustly determined. These values are projected, implying a higher intrinsic polarization fraction. In the western sectors, the foreground and in particular its $|L(\psi)|$ component increases rapidly with ψ , so our constant foreground approximation overestimates the downstream $|\Delta L|$; this systematic error is especially large in the SW sector, where even I can be estimated only in the near-downstream region. As the figure shows, the statistical errors are small in the synchrotron and dust regimes, but substantial in the intermediate, ~ 60 – 90 GHz frequency range.

Throughout the analyzed region, the polarization angle

$$\theta(L) \equiv \arg(L)/2 \quad (3)$$

(right-triangles in Fig. 2) lies in the $|\theta| \lesssim 30^\circ$ range, with implied magnetic fields roughly following the morphology of the extended lobes. However, small changes in the $\theta(\psi)$ behavior are identified at the FB edge in all four sectors: small but significant θ jumps at the two western sectors, and $\theta(\psi)$ trend reversals in the other two sectors. While the upstream θ_u (up-triangles in Fig. 3) can be determined robustly, it is difficult to measure the downstream angle θ_d of FB-associated emission, due to the strong, $\theta_f \simeq \theta_u$ foreground and off-edge projection effects. Indeed, either overestimating or underestimating the foreground would offset the measured θ_d towards

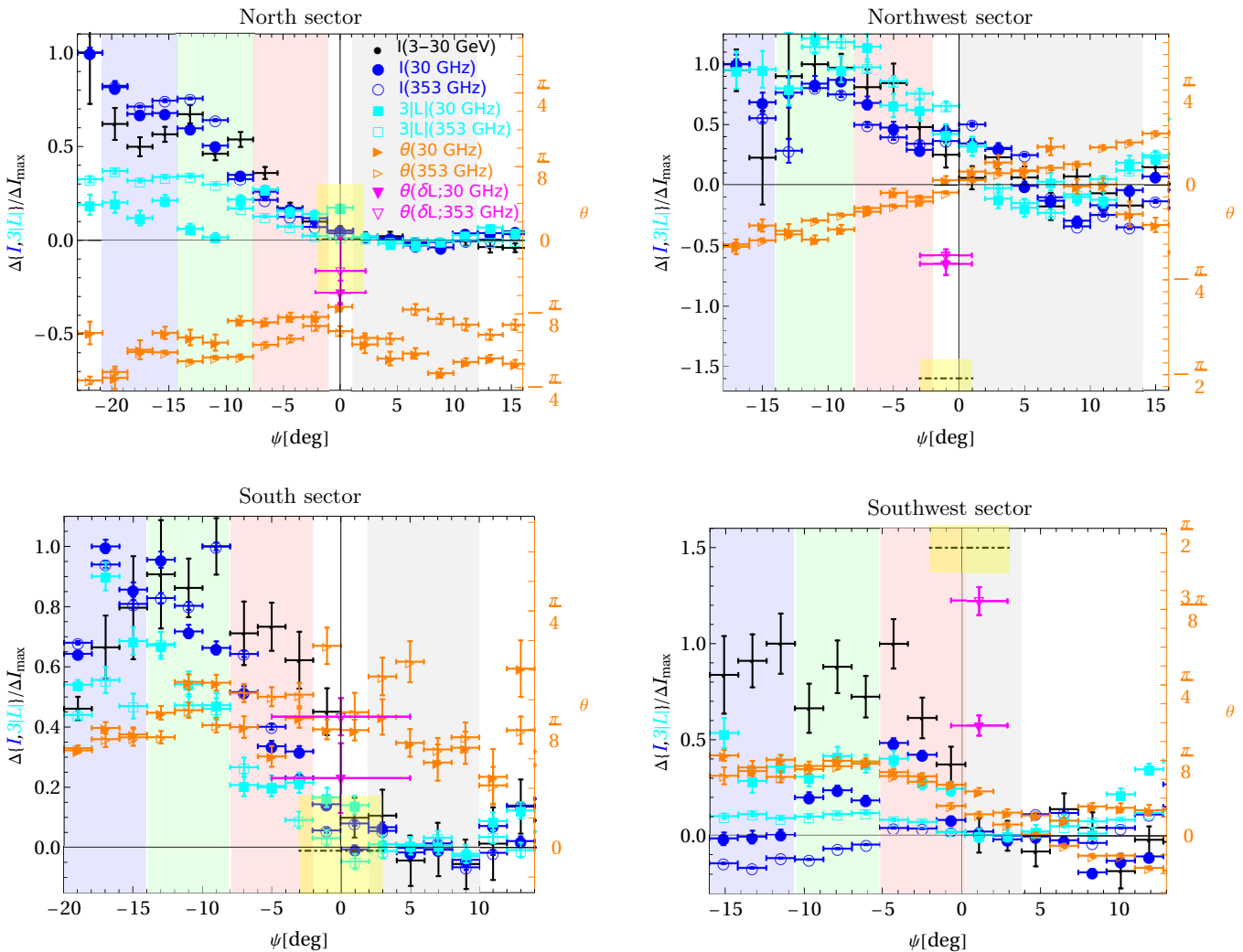


FIG. 2. Radial profiles (1σ error bars) of γ -ray (small black disks), 30 GHz synchrotron (filled symbols), and 353 GHz dust (empty symbols) emission, as a function of oriented angular distance ψ outside the FB edge, in the four (labeled) sectors. The total (I ; circles) and linearly polarized ($|L|$; cyan squares, multiplied by 3 for visibility) brightness excess above the foreground (based on the upstream, gray-shaded region), shown normalized to peak total brightness, rise abruptly downstream ($\psi \lesssim 0$); color shades define near (red), mid (green), and far (blue) downstream regions. The polarization angle θ (orange right-triangles, in *WMAP* conventions) trend changes near the $\psi \simeq 0$ edge; the angle of the δL jump across the edge (magenta down-triangles) is closer to the shock-normal angle θ_n (dot-dashed black line with yellow-shaded sector dispersion), especially in the west.

θ_f , and projection effects dilute the anticipated, edge-perpendicular polarization.

In Q - U space, the $L(\psi)$ trajectory shows a small δL jump at $\psi \simeq 0$ in all four sectors, thus providing a local, albeit noisy, estimate of the FB polarization angle with minimal projection effects. The corresponding $\theta(\delta L)$ angle, presented (in magneta) in Figs. 1 (solid lines show the inferred magnetic field orientation), 2 and 3 (down-triangles), lies approximately half-way between the upstream θ_u and the shock normal, θ_n (black dot-dashed lines in Figs. 2–3). This effect, more noticeable in the western sectors where θ_u and θ_n are farther apart, indicates that the near-downstream magnetic field is indeed aligned preferentially parallel to the shock front.

Thanks to their large extent on the sky, the FBs provide unique constraints on diverse physical processes,

ranging from cosmic-ray diffusion [*e.g.*, 13] to dust-grain alignment. The polarization angles of synchrotron and dust emission are similar to each other throughout the analyzed sectors, as often found in the magnetized interstellar medium; some differences are however seen, especially upstream of the FBs. Dust emission is thought to be preferentially polarized along the long grain axis, radiatively torqued perpendicular to the ambient magnetic field [23–26]. Our results constrain the alignment timescale as < 1 Myr (for $|\psi| =$ a few degrees downstream) under the extreme conditions at the FB outskirts: a highly ionized, hot (~ 0.5 keV electron temperature), and dilute (10^{-3} cm^{-3} density) gas, exposed to anisotropic, strong starlight [6].

There are interesting similarities between the polarized lobes and the FBs, invoking previous claims that the two

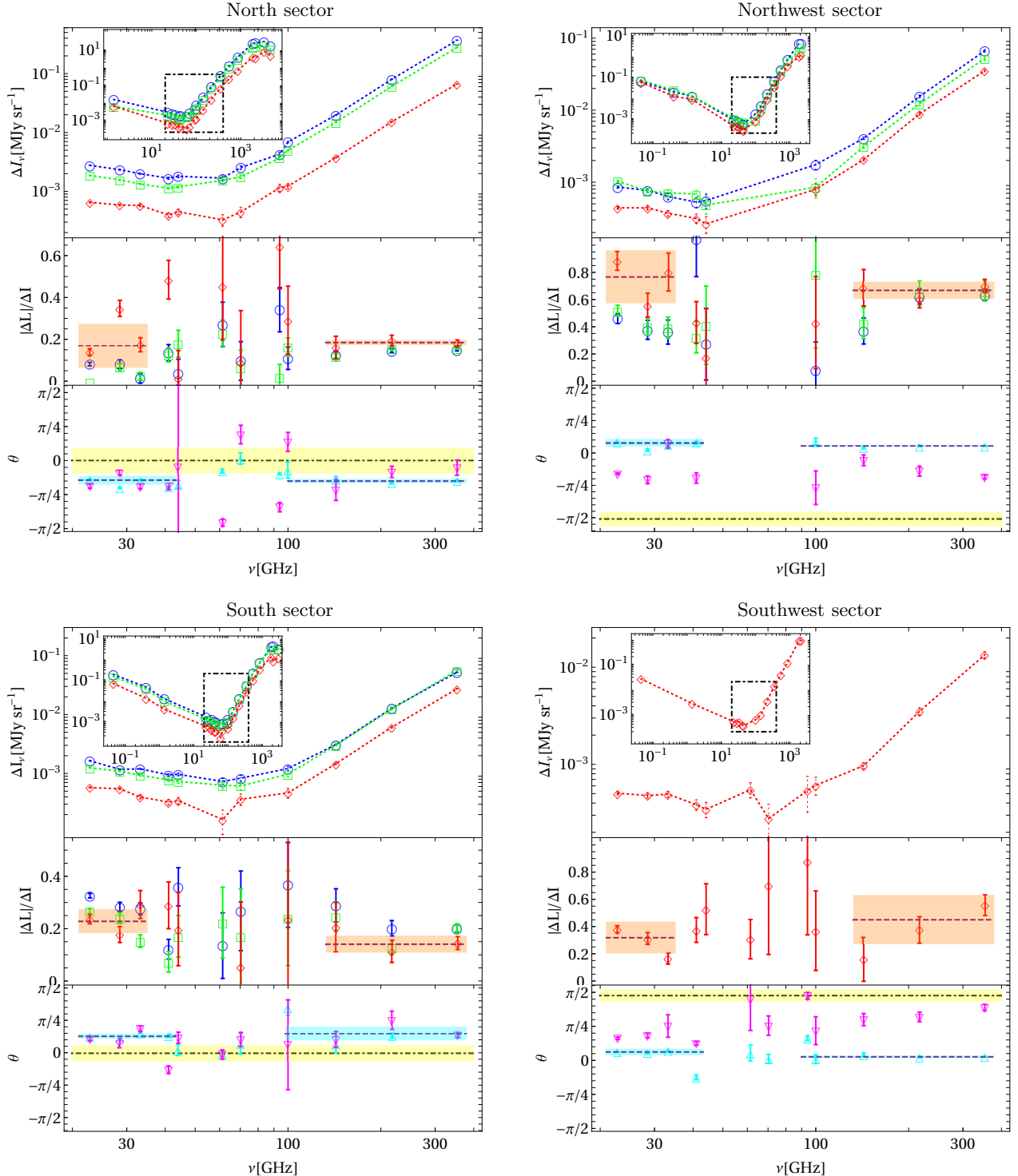


FIG. 3. Spectral analysis, in each sector (labeled panel composite), of the total brightness (top panels, with broader frequency-range [6] insets) and the linear polarization fraction (middle panels) of the excess in the near (red diamonds), mid (green squares) and far (blue circles) downstream regions, and of the polarization angles (bottom panels) θ_u upstream (cyan up triangles) and $\theta(\delta L)$ across the edge (magenta down triangles), compared to the edge-normal θ_n (dot-dashed line with yellow-shaded dispersion). The upstream and downstream regions are defined in Fig. 2. The mean near-downstream $|\Delta L|/\Delta I$ and upstream θ_u are similar in the synchrotron and dust regimes, shown (dashed lines with shaded dispersions) separately.

are complementary signatures of the same phenomenon. However, the above arguments, in particular the farther westward extent of the lobes reaching beyond the FB

edges, indicate that the lobes are not associated with the supersonic FBs or the outflows that produced them. The polarized FB signature found in this study is clearly

distinguished from the lobes, affirming this conclusion.

The $\gtrsim 40\%$ larger projected extent of the lobes, their large, $d \gtrsim 5.5$ kpc distance from the Sun inferred from their $|b| \lesssim 10^\circ$ depolarization [17], the similar curvature of their ridges and the GC spur [16], and the absence of localized lobe–FB collision signatures, indicate that they are large-scale structures emanating from the GC vicinity, and not objects lying in the FB background or foreground. Our results thus imply that the lobes are older (and so, more curved) than the FBs, encompassing the latter and being processed by their forward shocks.

The lobes were previously interpreted as arising from a

slow, $\gtrsim 100$ Myr star-formation-driven GC outflow, possibly linked to the $\sim 3 \times 10^7 M_\odot$ star-forming molecular gas ring [17]. However, their similarities to the FBs in terms of morphology, synchrotron signature, and $\gtrsim 10^{55}$ erg inferred energy, indicate that they are more likely to be the remnants of a collimated outburst from the SMBH, resembling but predating the FB outburst. If so, the lobes may well be the haze-like signature of the *ROSAT/eROSITA* [27, 28] bubbles: the larger, $b \gtrsim 80^\circ$ counterparts of the FBs.

I am grateful to Ilya Gurwich for helpful discussions. This research was supported by the Israel Science Foundation (Grant No. 2126/22).

-
- [1] F. K. Baganoff, Y. Maeda, M. Morris, M. W. Bautz, W. N. Brandt, W. Cui, J. P. Doty, E. D. Feigelson, G. P. Garmire, and S. H. Pravdo, *ApJ* **591**, 891 (2003), [arXiv:astro-ph/0102151 \[astro-ph\]](#).
- [2] J. Bland-Hawthorn and M. Cohen, *ApJ* **582**, 246 (2003), [arXiv:astro-ph/0208553 \[astro-ph\]](#).
- [3] G. Dobler, D. P. Finkbeiner, I. Cholis, T. Slatyer, and N. Weiner, *ApJ* **717**, 825 (2010), [arXiv:0910.4583 \[astro-ph.HE\]](#).
- [4] M. Su, T. R. Slatyer, and D. P. Finkbeiner, *ApJ* **724**, 1044 (2010), [arXiv:1005.5480 \[astro-ph.HE\]](#).
- [5] U. Keshet and I. Gurwich, *MNRAS* **480**, 223 (2018), [arXiv:1704.05070 \[astro-ph.HE\]](#).
- [6] U. Keshet, I. Gurwich, A. Lavi, D. Avitan, and T. Linnik, [arXiv e-prints](#), [arXiv:2311.08459 \(2023\)](#), [arXiv:2311.08459 \[astro-ph.HE\]](#).
- [7] G. Dobler, *ApJ* **760**, L8 (2012), [arXiv:1208.2690 \[astro-ph.HE\]](#).
- [8] Planck Collaboration, *A&A* **554**, A139 (2013), [arXiv:1208.5483 \[astro-ph.GA\]](#).
- [9] D. P. Finkbeiner, *ApJ* **614**, 186 (2004), [astro-ph/0311547](#).
- [10] W.-C. Huang, A. Urbano, and W. Xue, [ArXiv e-prints \(2013\)](#), [arXiv:1307.6862 \[hep-ph\]](#).
- [11] D. Hooper and T. R. Slatyer, *Physics of the Dark Universe* **2**, 118 (2013), [arXiv:1302.6589 \[astro-ph.HE\]](#).
- [12] M. Ackermann, A. Albert, W. B. Atwood, L. Baldini, J. Ballet, G. Barbiellini, D. Bastieri, R. Bellazzini, E. Bissaldi, R. D. Blandford, E. D. Bloom, E. Bottacini, T. J. Brandt, J. Bregeon, P. Bruel, R. Buehler, S. Buson, G. A. Caliandro, R. A. Cameron, M. Caragiulo, P. A. Caraveo, E. Cavazzuti, C. Cecchi, E. Charles, A. Chekhtman, J. Chiang, G. Chiaro, S. Ciprini, R. Claus, J. Cohen-Tanugi, J. Conrad, S. Cutini, F. D’Ammando, A. de Angelis, F. de Palma, C. D. Dermer, S. W. Digel, L. Di Venere, E. d. C. e. Silva, P. S. Drell, C. Favuzzi, E. C. Ferrara, W. B. Focke, A. Franckowiak, Y. Fukazawa, S. Funk, P. Fusco, F. Gargano, D. Gasparrini, S. Germani, N. Giglietto, F. Giordano, M. Giroletti, G. Godfrey, G. A. Gomez-Vargas, I. A. Grenier, S. Guiriec, D. Hadasch, A. K. Harding, E. Hays, J. W. Hewitt, X. Hou, T. Jogler, G. Jóhannesson, A. S. Johnson, W. N. Johnson, T. Kamae, J. Kataoka, J. Knödseder, D. Kocevski, M. Kuss, S. Larsson, L. Latronico, F. Longo, F. Loparco, M. N. Lovellette, P. Lubrano, D. Malyshev, A. Manfreda, F. Massaro, M. Mayer, M. N. Mazziotta, J. E. McEnery, P. F. Michelson, W. Mitthumsiri, T. Mizuno, M. E. Monzani, A. Morselli, I. V. Moskalenko, S. Murgia, R. Nemmen, E. Nuss, T. Ohsugi, N. Omodei, M. Orienti, E. Orlando, J. F. Ormes, D. Paneque, J. H. Panetta, J. S. Perkins, M. Pesce-Rollins, V. Petrosian, F. Piron, G. Pivato, S. Rainò, R. Rando, M. Razzano, S. Razzaque, A. Reimer, O. Reimer, M. Sánchez-Conde, M. Schaal, A. Schulz, C. Sgrò, E. J. Siskind, G. Spandre, P. Spinelli, L. Stawarz, A. W. Strong, D. J. Sunon, M. Tahara, H. Takahashi, J. B. Thayer, L. Tibaldo, M. Tinivella, D. F. Torres, G. Tosti, E. Troja, Y. Uchiyama, G. Vianello, M. Werner, B. L. Winer, K. S. Wood, M. Wood, and G. Zaharijas, *ApJ* **793**, 64 (2014), [arXiv:1407.7905 \[astro-ph.HE\]](#).
- [13] U. Keshet and I. Gurwich, *ApJ* **840**, 7 (2017), [arXiv:1611.04190 \[astro-ph.HE\]](#).
- [14] S. Mondal, U. Keshet, K. C. Sarkar, and I. Gurwich, *MNRAS* **514**, 2581 (2022), [arXiv:2109.03834 \[astro-ph.HE\]](#).
- [15] K. C. Sarkar, S. Mondal, P. Sharma, and T. Piran, *ApJ* **951**, 36 (2023), [arXiv:2211.12967 \[astro-ph.HE\]](#).
- [16] D. I. Jones, R. M. Crocker, W. Reich, J. Ott, and F. A. Aharonian, *ApJ* **747**, L12 (2012), [arXiv:1201.4491 \[astro-ph.HE\]](#).
- [17] E. Carretti, R. M. Crocker, L. Staveley-Smith, M. Haverkorn, C. Purcell, B. M. Gaensler, G. Bernardi, M. J. Kesteven, and S. Poppi, *Nature* **493**, 66 (2013), [arXiv:1301.0512 \[astro-ph.GA\]](#).
- [18] B. Gold, N. Odegard, J. L. Weiland, R. S. Hill, A. Kogut, C. L. Bennett, G. Hinshaw, X. Chen, J. Dunkley, M. Halpern, N. Jarosik, E. Komatsu, D. Larson, M. Limon, S. S. Meyer, M. R. Nolta, L. Page, K. M. Smith, D. N. Spergel, G. S. Tucker, E. Wollack, and E. L. Wright, *ApJS* **192**, 15 (2011), [arXiv:1001.4555 \[astro-ph.GA\]](#).
- [19] G. Dobler, *ApJ* **750**, 17 (2012), [arXiv:1109.4418 \[astro-ph.GA\]](#).
- [20] Planck Collaboration, N. Aghanim, Y. Akrami, M. I. R. Alves, M. Ashdown, J. Aumont, C. Baccigalupi, M. Ballardini, A. J. Banday, R. B. Barreiro, N. Bartolo, S. Basak, K. Benabed, J. P. Bernard, M. Bersanelli, P. Bielewicz, J. J. Bock, J. R. Bond, J. Borrill, F. R. Bouchet, F. Boulanger, A. Bracco, M. Bucher, C. Burigana, E. Calabrese, J. F. Cardoso, J. Carron, R. R.

- Chary, H. C. Chiang, L. P. L. Colombo, C. Combet, B. P. Crill, F. Cuttaia, P. de Bernardis, G. de Zotti, J. Delabrouille, J. M. Delouis, E. Di Valentino, C. Dickinson, J. M. Diego, O. Doré, M. Douspis, A. Ducout, X. Dupac, G. Efstathiou, F. Elsner, T. A. Enßlin, H. K. Eriksen, E. Falgarone, Y. Fantaye, R. Fernandez-Cobos, K. Ferrière, F. Finelli, F. Forastieri, M. Frailis, A. A. Fraisse, E. Franceschi, A. Frolov, S. Galeotta, S. Galli, K. Ganga, R. T. Génova-Santos, M. Gerbino, T. Ghosh, J. González-Nuevo, K. M. Górski, S. Gratton, G. Green, A. Gruppuso, J. E. Gudmundsson, V. Guillet, W. Handley, F. K. Hansen, G. Helou, D. Herranz, E. Hivon, Z. Huang, A. H. Jaffe, W. C. Jones, E. Keihänen, R. Keskitalo, K. Kiiveri, J. Kim, N. Krachmalnicoff, M. Kunz, H. Kurki-Suonio, G. Lagache, J. M. Lamarre, A. Lasenby, M. Lattanzi, C. R. Lawrence, M. Le Jeune, F. Levrier, M. Liguori, P. B. Lilje, V. Lindholm, M. López-Cañiego, P. M. Lubin, Y. Z. Ma, J. F. Macías-Pérez, G. Maggio, D. Maino, N. Mandolesi, A. Mangilli, A. Marcos-Caballero, M. Maris, P. G. Martin, E. Martínez-González, S. Matarrese, N. Mauri, J. D. McEwen, A. Melchiorri, A. Mennella, M. Migliaccio, M. A. Miville-Deschênes, D. Molinari, A. Moneti, L. Montier, G. Morgante, A. Moss, P. Natoli, L. Pagano, D. Paoletti, G. Patanchon, F. Perrotta, V. Pettorino, F. Piacentini, L. Polastri, G. Polenta, J. L. Puget, J. P. Rachen, M. Reinecke, M. Remazeilles, A. Renzi, I. Ristorcelli, G. Rocha, C. Rosset, G. Roudier, J. A. Rubiño-Martín, B. Ruiz-Granados, L. Salvati, M. Sandri, M. Savelainen, D. Scott, C. Sirignano, R. Sunyaev, A. S. Suur-Uski, J. A. Tauber, D. Tavagnacco, M. Tenti, L. Toffolatti, M. Tomasi, T. Trombetti, J. Valiviita, F. Vansyngel, B. Van Tent, P. Vielva, F. Villa, N. Vittorio, B. D. Wandelt, I. K. Wehus, A. Zacchei, and A. Zonca, *A&A* **641**, A12 (2020), [arXiv:1807.06212 \[astro-ph.GA\]](#).
- [21] The lobes were not shown to sharply cut off at the putative edges and may be more extended than claimed [17].
- [22] S. d. Serego Alighieri, *Experimental Astronomy* **43**, 19 (2017).
- [23] A. Z. Dolginov and I. G. Mitrofanov, *Ap&SS* **43**, 291 (1976).
- [24] B. T. Draine and J. C. Weingartner, *ApJ* **480**, 633 (1997), [arXiv:astro-ph/9611149 \[astro-ph\]](#).
- [25] T. Hoang and A. Lazarian, *MNRAS* **388**, 117 (2008), [arXiv:0707.3645 \[astro-ph\]](#).
- [26] A. Lazarian, *J. Quant. Spec. Radiat. Transf.* **106**, 225 (2007), [arXiv:0707.0858 \[astro-ph\]](#).
- [27] Y. Sofue, *ApJ* **540**, 224 (2000), [arXiv:astro-ph/9912528 \[astro-ph\]](#).
- [28] P. Predehl, R. A. Sunyaev, W. Becker, H. Brunner, R. Burenin, A. Bykov, A. Cherepashchuk, N. Chugai, E. Churazov, V. Doroshenko, N. Eismont, M. Freyberg, M. Gilfanov, F. Haberl, I. Khabibullin, R. Krivonos, C. Maitra, P. Medvedev, A. Merloni, K. Nandra, V. Nazarov, M. Pavlinsky, G. Ponti, J. S. Sanders, M. Sasaki, S. Sazonov, A. W. Strong, and J. Wilms, *Nature* **588**, 227 (2020), [arXiv:2012.05840 \[astro-ph.GA\]](#).